AGU PUBLICATIONS

Paleoceanography

RESEARCH ARTICLE
10.1002/2017PA003118

Key Points:
- The delta^{13}C and delta^{18}O in the deep Southwest Atlantic and Southwest Pacific below 2.5 km were more dissimilar during the LGM and through most of the deglaciation
- Isotopic changes in the deepest Southwest Pacific led the Southwest Atlantic through the deglaciation
- When GNAIW shoaled above the Drake Passage sill depth, this interior North Atlantic water mass was prevented from entering the Southern Ocean

Supporting Information:
- Supporting Information S1
- Movie S1
- Movie S2

Correspondence to:
E. L. Sikes,
sikes@marine.rutgers.edu

Citation:
Sikes, E. L., Allen, K. A., & Lund, D. C. (2017). Enhanced δ^{13}C and δ^{18}O differences between the South Atlantic and South Pacific during the last glaciation: The deep gateway hypothesis. *Paleoceanography*, *32*. https://doi.org/10.1002/2017PA003118

Received 9 MAR 2017
Accepted 1 SEP 2017
Accepted article online 12 SEP 2017

Enhanced δ^{13}C and δ^{18}O Differences Between the South Atlantic and South Pacific During the Last Glaciation: The Deep Gateway Hypothesis

Elisabeth L. Sikes[1], Katherine A. Allen[2], and David C. Lund[3]

[1]Institute of Marine and Coastal Sciences, State University of New Jersey, Rutgers, New Brunswick, NJ, USA, [2]School of Earth and Climate Sciences, University of Maine, Orono, ME, USA, [3]Department of Marine Sciences, University of Connecticut Avery Point, Groton, CT, USA

Abstract Enhanced vertical gradients in benthic foraminiferal δ^{13}C and δ^{18}O in the Atlantic and Pacific during the last glaciation have revealed that ocean overturning circulation was characterized by shoaling of North Atlantic sourced interior waters; nonetheless, our understanding of the specific mechanisms driving these glacial isotope patterns remains incomplete. Here we compare high-resolution depth transects of *Cibicidoides* spp. δ^{13}C and δ^{18}O from the Southwest Pacific and the Southwest Atlantic to examine relative changes in northern and southern sourced deep waters during the Last Glacial Maximum (LGM) and deglaciation. During the LGM, our transects show that water mass properties and boundaries in the South Atlantic and Pacific were different from one another. The Atlantic between ~1.0 and 2.5 km was more than 1‰ enriched in δ^{13}C relative to the Pacific and remained more enriched through the deglaciation. During the LGM, Atlantic δ^{18}O was ~0.5‰ more enriched than the Pacific, particularly below 2.5 km. This compositional difference between the deep portions of the basins implies independent deep water sources during the glaciation. We attribute these changes to a "deep gateway" effect whereby northern sourced waters shallower than the Drake Passage sill were unable to flow southward into the Southern Ocean because a net meridional geostrophic transport cannot be supported in the absence of a net east-west circumpolar pressure gradient above the sill depth. We surmise that through the LGM and early deglaciation, shoaled northern sourced waters were unable to escape the Atlantic and contribute to deep water formation in the Southern Ocean.

1. Introduction: Understanding the Glacial Ocean

Ocean circulation plays a key role in regulating atmospheric CO_2 concentrations on glacial-interglacial timescales, with a combination of changes in ocean overturning, stratification, biological nutrient uptake, and carbonate compensation required to explain the observed glacial decrease of ~80 ppm in atmospheric CO_2 (e.g., Boyle, 1988; Sigman et al., 2010). The formation of deep water in the North Atlantic ventilates the deep ocean today, and changes in this Atlantic Meridional Overturning Circulation (AMOC) during glacial intervals likely contributed to the reduction of atmospheric CO_2 in the past (e.g., Toggweiler, 1999).

The Southern Ocean is also an important area for ocean-atmosphere gas exchange. Here deep water exported from the North Atlantic is modified and ventilated during the formation of Antarctic water masses (e.g., Talley, 2013). Changes in the Southern Ocean such as the documented expansion of sea ice around Antarctica and the northward movement of fronts (Gersonde et al., 2005; Howard & Prell, 1992; Sikes et al., 2009) have been proposed as mechanisms for trapping CO_2 in the glacial ocean (Ferrari et al., 2014; Sigman et al., 2010). There is general agreement that during the Last Glacial Maximum (LGM) changes in both thermohaline circulation and Southern Ocean air-sea-ventilation dynamics affected atmosphere-ocean CO_2 partitioning, but the details of these processes and their relative importance are still a matter of ongoing debate.

1.1. Modern Circulation in the Southern Ocean

The formation of North Atlantic Deep Water (NADW) is an essential process driving modern AMOC. Today, NADW enters the Southern Ocean through the South Atlantic, joining deep waters flowing through the Drake Passage. The resulting combination of Pacific, Indian, and Atlantic deep waters is transported eastward as Circumpolar Deep Water (CDW) in the Antarctic Circumpolar Current (ACC). In the Pacific sector, carbon-rich CDW upwells in response to density and wind-driven divergence around Antarctica. The

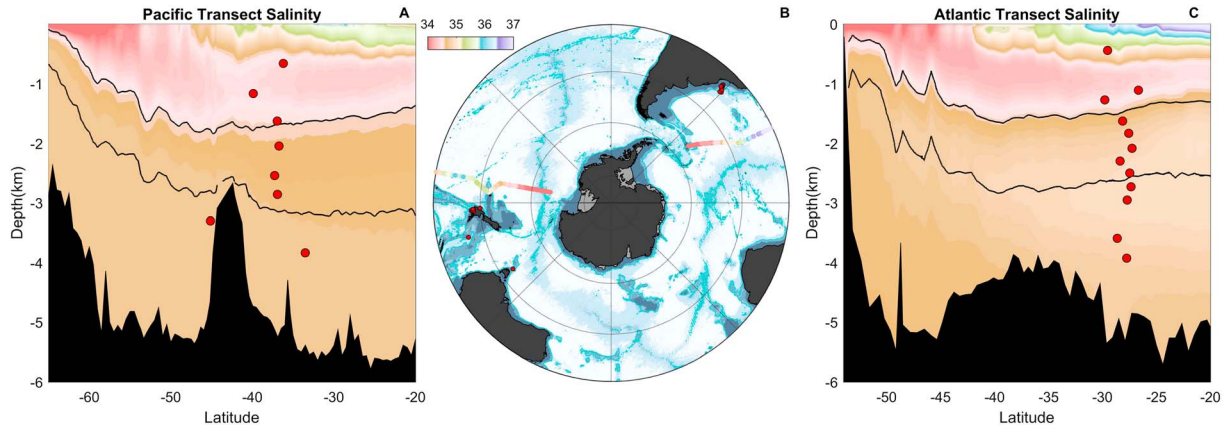

Figure 1. Southern Hemisphere bathymetry and water mass structure. (a) South Pacific salinity profile along World Ocean Circulation Experiment (WOCE) P15 with core depths projected onto the profile. (b) Core locations and schematic representation of water mass salinity transects. Cores with data presented in this paper are indicated by red circles. The 2.5 km bathymetric contour is highlighted in green. (c) South Atlantic salinity profile along WOCE A16, with core depths from the Brazil Margin projected onto the profile. On the vertical transects the isoneutral density surface, $\gamma^N = 27.8$ is represented by the upper black line and $\gamma^N = 28.04$ kg/m^3 by the lower black line. The 28.04 kg/m^3 is approximately the densest isopycnal crossing Drake Passage at sill depth, 27.8 kg/m^3 is the core of the IDW/PDW, and 28.04 kg/m^3 is the core of the NADW today (see Talley, 2013, and references therein).

subsequent conversion of the less dense layers of CDW or Upper CDW (UCDW) to intermediate water by air-sea fluxes (i.e., addition of freshwater and heat) forms an important component of the upward limb of the thermohaline overturning circulation (Talley, 2013). These waters move northward from the Polar Front (PF) and lose CO_2 to the atmosphere before they sink to form Antarctic Intermediate Water (AAIW) and Subantarctic Mode Water (SAMW) near the Subantarctic Front (SAF) and the Subtropical Front (STF), respectively (Belkin & Gordon, 1996; Orsi et al., 1995). Both AAIW (800–1500 m) and SAMW (400–800 m) flow northward beneath warmer and saltier subtropical surface waters of the Pacific Ocean. South of the Polar Front, upwelled denser layers or Lower CDW (LCDW), the core of which is composed of NADW in both the Atlantic and Pacific, flow southward where buoyancy loss and sea ice formation creates deeper Antarctic Bottom Water (AABW). In the Atlantic, AABW forms in the Weddell Sea, where NADW upwells and mixes with shelf water (Orsi et al., 1999; Talley, 2013) increasing its density (AABW neutral density, $\gamma^N > 28.3$ kg/m^3, Figure 1). An important subtlety in the Pacific sector of the Southern Ocean is that UCDW has a significant component of Pacific Deep Water (PDW) and Indian Deep Water (IDW), and this water upwells north of LCDW, making PDW/IDW the primary source of northward flowing shallow water masses in the Pacific today (Marshall & Speer, 2012; Talley, 2013) (Figure 2a). UCDW also forms a significant component of the flow through the Drake Passage (Talley, 2013). The Southern Ocean is bounded to the north by the STF, which is the southern limit of the subtropical gyres. This important boundary and the location of all the major fronts in the Southern Ocean are determined by the winds, and along with the broad eastward flow of the ACC, they are also steered by bathymetry.

Past circulation in the Southern Ocean can be inferred from geochemical tracers, including $\delta^{13}C$ (Figure 1 and Figures S1–S3 in the supporting information; see also discussion in the supporting information). The $\delta^{13}C$ signatures in subsurface waters are controlled by a balance of atmospheric exchange and interior respiration modulated by the overturning circulation (for a review see Sigman et al., 2010). The $\delta^{13}C$ of deep waters reflect the cumulative effects of processes that add or remove dissolved inorganic carbon (DIC) from seawater while fractionating its isotopic composition; thus, the $\delta^{13}C$ of DIC reflects preformed nutrients, air-sea CO_2 exchange, and organic matter respiration at depth (addition of DIC and nutrients) (Curry et al., 1988; Lynch-Stieglitz et al., 1994, 2007; Sallée et al., 2010; Takahashi et al., 2009). Notably, because of the dominating influence of air-sea exchange, the $\delta^{13}C$ of intermediate waters exiting the Southern Ocean are understood to primarily be a tracer for air-sea processes rather than a tracer for nutrients or respired DIC (Lynch-Stieglitz et al., 1994), as it is used in subsurface waters elsewhere (Lynch-Stieglitz et al., 2007). During transport in the shallow subsurface interior, these water masses retain the carbon isotopic signal of atmospheric gas exchange in the Southern Ocean that is a function of wind strength, position, and time of exposure at the surface (Sallée et al., 2010; Takahashi et al., 2009). Consequently, the $\delta^{13}C$ of Southern

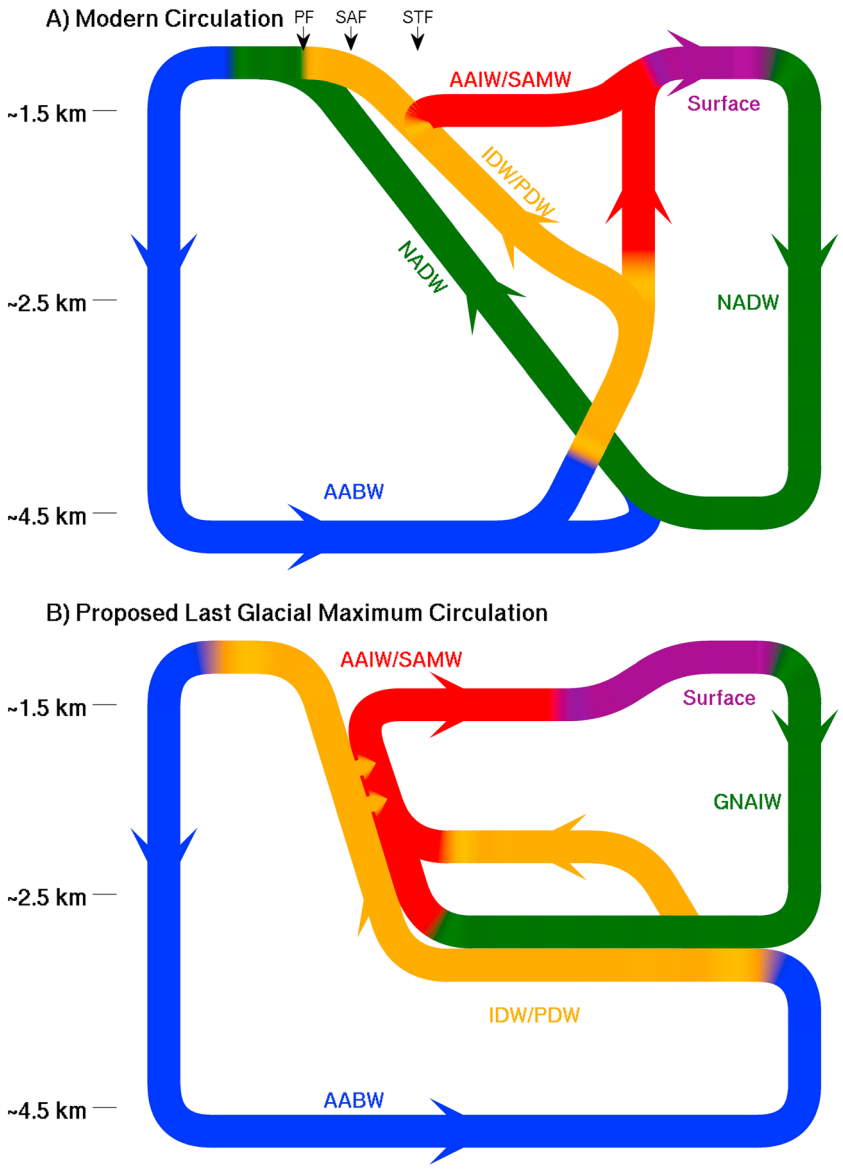

Figure 2. Overturning circulation schematics, two-dimensional view. (a) Modern circulation as depicted in Talley (2013). Approximate locations of the major fronts that separate interior water formation zones are indicated by arrows, Polar Front (PF), Subantarctic Front (SAF), and the Subtropical Front (STF). The STF is the northern boundary of the Southern Ocean. (b) Hypothesized overturning circulation for the LGM depicting both Atlantic and Pacific overturning cells. Colors represent the water masses as follows: blue = AABW, green = NADW/GNAIW, orange = PDW/IDW, red = AAIW/SAMW, and purple = surface low-latitude, primarily Atlantic. Note that in the modern circulation the two oceans are fundamentally intertwined through NADW transport and conversion through upwelling in the Southern, Indian, and Pacific Oceans. In the LGM, the oceans are more separate, connecting only through the conversion of PDW/IDW to intermediate waters and flow through Drake Passage that was reduced in the LGM.

Ocean water masses are distinct, with the relatively positive $\delta^{13}C$ of SAMW and AAIW reflecting CO_2 exchange with the cold polar atmosphere (e.g., Bostock et al., 2010; Charles et al., 1993), whereas the lower $\delta^{13}C$ values for deep waters indicate the ^{13}C-depleted respired CO_2 that accumulates during isolation from the atmosphere (Curry et al., 1988).

1.2. Past Reconstructions of Glacial Circulation: Focus on the Southern Ocean

The structure and source of interior water masses in the past can be constrained by the record of seawater $\delta^{13}C$ and $\delta^{18}O$ preserved in the calcium carbonate tests of benthic foraminifera (Charles & Fairbanks, 1992;

Charles et al., 2010; Curry & Oppo, 2005; Hodell et al., 2003; Mackensen, 2012; Ninnemann & Charles, 2002) (Figure S2). The $\delta^{13}C$ profiles provide a means of tracking atmosphere CO_2 exchange or isolation and addition of isotopically light carbon via the biologic pump (also called the soft tissue pump). The speciation of DIC in the mixed layer can also impact the shape of $\delta^{13}C$ profiles by influencing the rate at which the DIC pool's composition is reset (Galbraith et al., 2015). Nonetheless, $\delta^{13}C$ profiles provide valuable insight into ocean storage of respired CO_2, particularly where complementary oxygenation and/or [CO_3^{2-}] data are available (Allen et al., 2015; Yu et al., 2008). The $\delta^{18}O$ of foraminiferal calcite is a function of temperature and seawater $\delta^{18}O$, which is linked to salinity in the surface ocean via preferential evaporation of fresh, isotopically light water (LeGrande & Schmidt, 2006) and to global ice volume via the net accumulation of isotopically light precipitation on land (Shackleton, 1967). Once water is subducted below the sea surface, $\delta^{18}O$ is not affected by any process other than mixing, and thus, it acts as a conservative water mass tracer that is linked to seawater density (Adkins, 2013; Lynch-Stieglitz et al., 2007).

Changes in AMOC during the last glaciation could have contributed to greater sequestration of CO_2 in the ocean through a combination of effects. In the Atlantic, multiple lines of geochemical evidence paint a picture of dramatic changes in AMOC geometry characterized by the shoaling of NADW to above 2 km (GNAIW, Glacial North Atlantic Intermediate Water) (e.g., Boyle, 1988; Boyle & Keigwin, 1987; Curry & Oppo, 2005; Gherardi et al., 2009; Lund et al., 2011, 2015; McManus et al., 2004; Rutberg et al., 2000). Although there is some evidence of small amounts of deep water formation in the North Atlantic (Keigwin & Swift, 2017) waters of North Atlantic origin were largely absent below depths of ~2 km and so, water masses sourced from the Antarctic expanded in volume (Curry & Oppo, 2005; Lund et al., 2011, 2015; Lynch-Stieglitz et al., 2007). In the South Pacific, $\delta^{13}C$ evidence indicates the geochemical divide shoaled to between 600 and 1100 m (Sikes, Elmore, et al., 2016). Pacific $\Delta^{14}C$ and $\delta^{13}C$ reconstructions indicate older and less ventilated deep water during the Last Glacial Maximum (LGM), particularly at UCDW depths (Burke & Robinson, 2012; Curry et al., 1988; McCave et al., 2008; Ronge et al., 2016; Sarnthein et al., 2013; Sikes, Cook, et al., 2016; Sikes, Elmore, et al., 2016; Sikes et al., 2000; Skinner et al., 2015).

Published South Atlantic-South Pacific comparisons of LGM $\delta^{13}C$ indicate larger differences in geochemical signatures between these basins during the LGM (Charles et al., 2010; Hu et al., 2016; Ninnemann & Charles, 2002). Depth profiles suggest that the deep geochemical divide in the Pacific (as indicated by $\delta^{13}C$) was around 1000 m shallower than in the Atlantic (Hodell et al., 2003; McCave et al., 2008; Sikes, Elmore, et al., 2016) with Pacific UCDW $\delta^{13}C$ ~1‰ more depleted than modern and ~1‰ depleted relative to the Atlantic (McCave et al., 2008; Sikes, Elmore, et al., 2016). Estimates of paleodensity suggest that these geochemical divides may not necessarily correspond to physical stratification (Roberts et al., 2015). The isolation of AABW and LCDW maintained by benthic sills has been put forward to explain the difference in deepest waters (McCave et al., 2008). Existing time series from abyssal depths suggest that water at 3.0 to 3.6 km in the East Pacific had very similar glacial-interglacial $\delta^{13}C$ offsets over the last 500 ka to those in the northern Cape Basin at ~4.0 km, while below 4.6 km in the southern Cape Basin, waters were primarily more depleted (Ullermann et al., 2016).

Published comparisons of regional $\delta^{18}O$ stacks have demonstrated that the effects of the termination on the deep ocean were not globally synchronous, with deep North Atlantic isotope depletion below 2 km leading the deep Pacific (Stern & Lisiecki, 2014). Similarly, for intermediate waters the deglaciation was not synchronous, with the South Atlantic having the earliest termination onset (Stern & Lisiecki, 2014). Outside of stacked analyses, previous interbasin comparisons have typically focused either on single cores or glacial-interglacial time slices. Here we use two depth transects composed of independently dated, high-resolution time series with high depth resolution (one core every ~300 m between ~0.5 km and 4 km depth), to examine interbasin differences during the LGM and the deglacial. In particular, we seek to examine the depth-specific differences between the Southwest Atlantic and Southwest Pacific basins that stacked data or comparisons across depths may not resolve.

2. Materials and Methods

2.1. Core Locations and Stratigraphy

This work compares previously published benthic foraminiferal stable isotopic results from two depth transects, one located on the Brazil Margin in the South Atlantic (Lund et al., 2015) and another from New

Zealand in the Southwest Pacific (Sikes, Elmore, et al., 2016). The principal portion of the Pacific depth transect is composed of five jumbo piston cores collected from the Bay of Plenty, north and east of the North Island of New Zealand, augmented with deeper cores from the Tasman Sea and South Tasman Rise (Figure S1). Age control is largely tephra based in the Pacific cores as previously presented in the supporting information accompanying Sikes, Elmore, et al. (2016) (see also discussion in the supporting information (Lowe et al., 2013; Reimer et al., 2013; Samson et al., 2005; Shane et al., 2006; Sikes & Guilderson, 2016; Vandergoes et al., 2013)). Crucial to the tightness of stratigraphic control in the Pacific transect, there is a tephra associated with each of the climatic intervals examined in vertical profile (see discussion in the supporting information (Lowe et al., 2013; Reimer et al., 2013; Shane et al., 2006; Vandergoes et al., 2013)). In the Atlantic cores, stratigraphy is based on high-resolution ^{14}C dating (Lund et al., 2015). We estimate that any changes to surface reservoir ages differing from modern determined for the Brazil Margin would add an additional error on the order of ±360 years through the deglaciation which is substantially less than the length of the time slice averages (Angulo et al., 2005; Balmer et al., 2016). Sample preparation and isotopic analyses are as described in the original publications (Lund et al., 2015; Sikes, Elmore, et al., 2016) (see discussion in the supporting information (Elmore, 2009)).

In the Pacific, our depth transect intersects the major interior water masses from the deepest (AABW, LCDW, and UCDW) to the shallower water masses, SAMW and AAIW, that form in the northern regions of the Southern Ocean and penetrate well northward of the study sites (see discussion in the supporting information (Bostock et al., 2010; Chiswell et al., 2015; Schmittner et al., 2013). In the Southwest Atlantic, our depth transect also intersects the major interior water masses, with the presence of southward flowing NADW well documented (Figure S3) (e.g., Talley, 2013). Northward flowing AABW, AAIW, and SAMW are present above and below NADW (Talley, 2013). Formation of AABW in the Atlantic occurs in the Weddell Sea and flows northward, below NADW well into the Southwest Atlantic, reaching as far north as the equator (Orsi et al., 1999). Today, AABW that formed in the Ross Sea flows through fractures in the Pacific Antarctic Ridge moving northward to fill the deep southwestern Pacific including the New Zealand region (Talley, 2013). Any changes in AABW end-member composition from the Atlantic during the LGM should be obvious at the Brazil Margin sites (Figure 1) (Lund et al., 2015; Tessin & Lund, 2013). As a result, our "dueling transects" provide a high-resolution, proximal cross-sectional comparison of southern sourced water masses in the Pacific versus those in the Atlantic Ocean throughout the last glaciation and deglaciation (Figure 1). Modern $\delta^{13}C$ of seawater DIC is faithfully reproduced by late Holocene *Cibicidoides* depth profiles, demonstrated by a detailed comparison in the Pacific study area (Figures S1 and S2; see also discussion in the supporting information (Duplessy et al., 1984; Gruber et al., 1999; Mackensen, 2012; Mackensen et al., 1993; McCorkle & Keigwin, 1994)).

2.2. Contour Plot Generation and Calculation of Time Slice Averages

The $\delta^{13}C$ and $\delta^{18}O$ contour plots include benthic foraminiferal data from all sample intervals in all cores. Visualization of the benthic foraminiferal data is enhanced by the generation of a smoothed contour plot based on the total suite of cores. To facilitate the comparison of Atlantic and Pacific benthic foraminiferal data, a common grid in time and depth is required. The gridding process, using standard interpolation/visualization packages, was as follows: The data from each core were linearly interpolated to a common time coordinate with a resolution of 500 years. Then data in the resulting time series that were outside the time range of the core were extrapolated using a linear nearest-neighbor method. The higher-vertical-resolution Atlantic data were then linearly interpolated to the lower vertical resolution Pacific data. The uniformly gridded data were contoured at 0.1‰ intervals using the "contourf" function in MATLAB, which minimizes high-frequency variability. Core chronologies in this study are largely based on tephra stratigraphy or radiocarbon dates (without $\delta^{18}O$ tuning or matching), allowing us to use vertical and interbasin $\delta^{18}O$ differences to isolate and assess temperature and salinity variability.

Averages of benthic foraminiferal $\delta^{13}C$ and $\delta^{18}O$ values were calculated for key climatic time intervals identified by independent paleoclimate records (intervals indicated by the shaded panels in Figure 3). This averaging allows better examination of the vertical structure for these key climatic intervals: Glacial (19–23 ka), Heinrich Stadial 1 (HS1: 14.5–17.5 ka), Antarctic Cold Reversal (ACR; 12.9–14.5 ka), Younger Dryas (YD; 11–12.8 ka), and Holocene (0–10.5 ka).

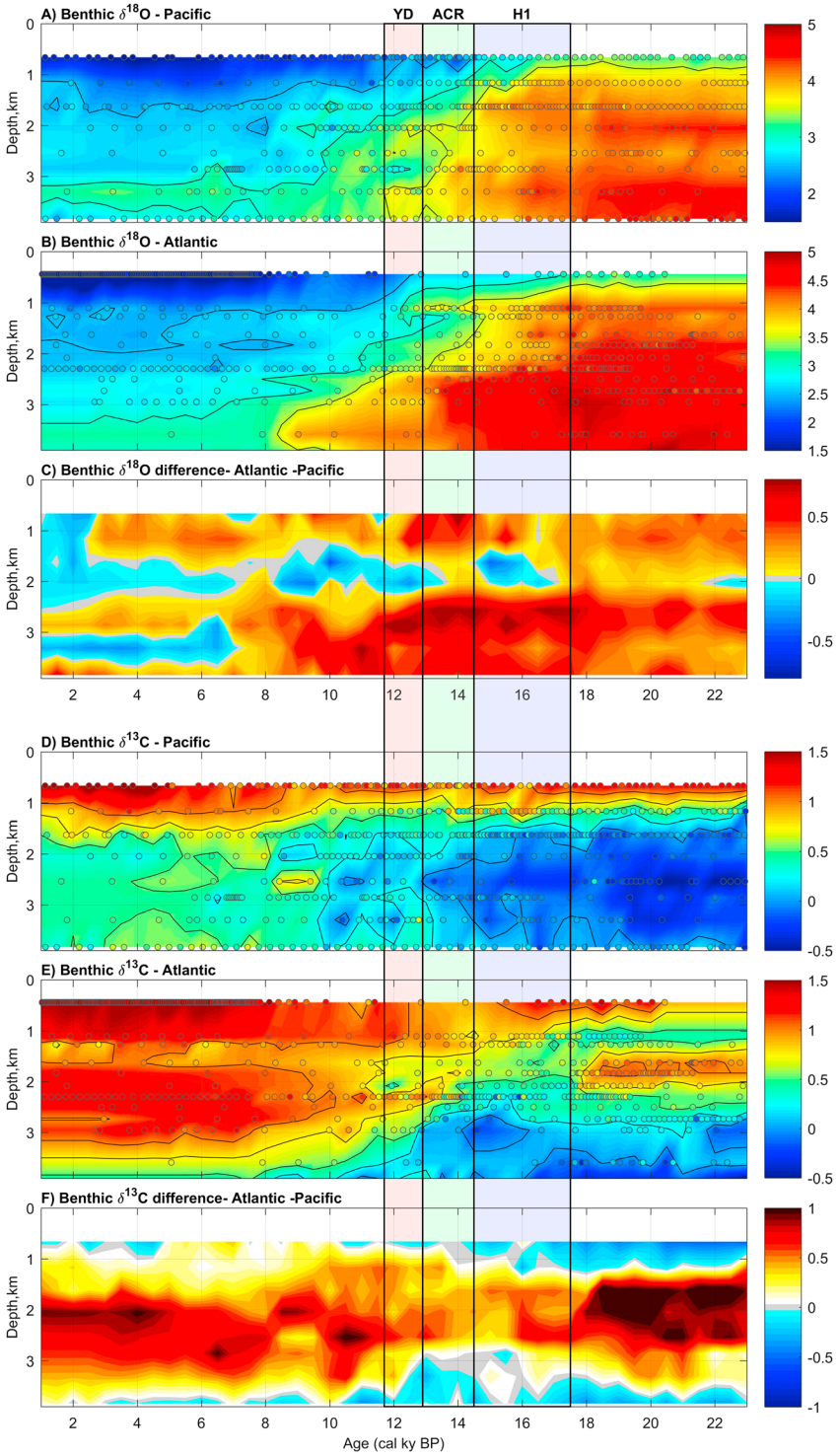

Figure 3. Contoured depth-time plots of stable isotopes on the Brazil Margin and in the Southwest Pacific and since the last glaciation. (a) Contour diagram of Southwest Pacific benthic $\delta^{18}O$ during the last deglaciation. Individual data points are shown as circles. (b) Contour diagram of Brazil Margin benthic $\delta^{18}O$ during the last deglaciation. Individual data points are shown as circles. (c) Contour diagram of Atlantic-Pacific benthic $\delta^{18}O$ differences. Note that the zone of smallest difference between the basins is centered on 2 km that persists from the LGM through the deglaciation. (d) Contour diagram of benthic $\delta^{13}C$ during the last deglaciation. Note the strong chemical stratification between 25 ka and 17 ka, indicated by a sharp, shallow $\delta^{13}C$ gradient, and the deep enrichment through the termination, ending with more positive $\delta^{13}C$ values below 2 km in the Holocene. (e) Contour diagram of Brazil Margin benthic $\delta^{13}C$ during the last deglaciation. Note the strong $\delta^{13}C$ enrichment narrowly centered on 1.8 km in the LGM, the loss of that in the deglaciation, and the deeper and broader $\delta^{13}C$ enrichment centered on 2.5 km in the Holocene. (f) Contour diagram of Atlantic-Pacific benthic $\delta^{13}C$ differences. Note that the greatest difference between basins was during the LGM and was centered at ~1.8 km, whereas in the Holocene this difference is centered at 2.5 km.

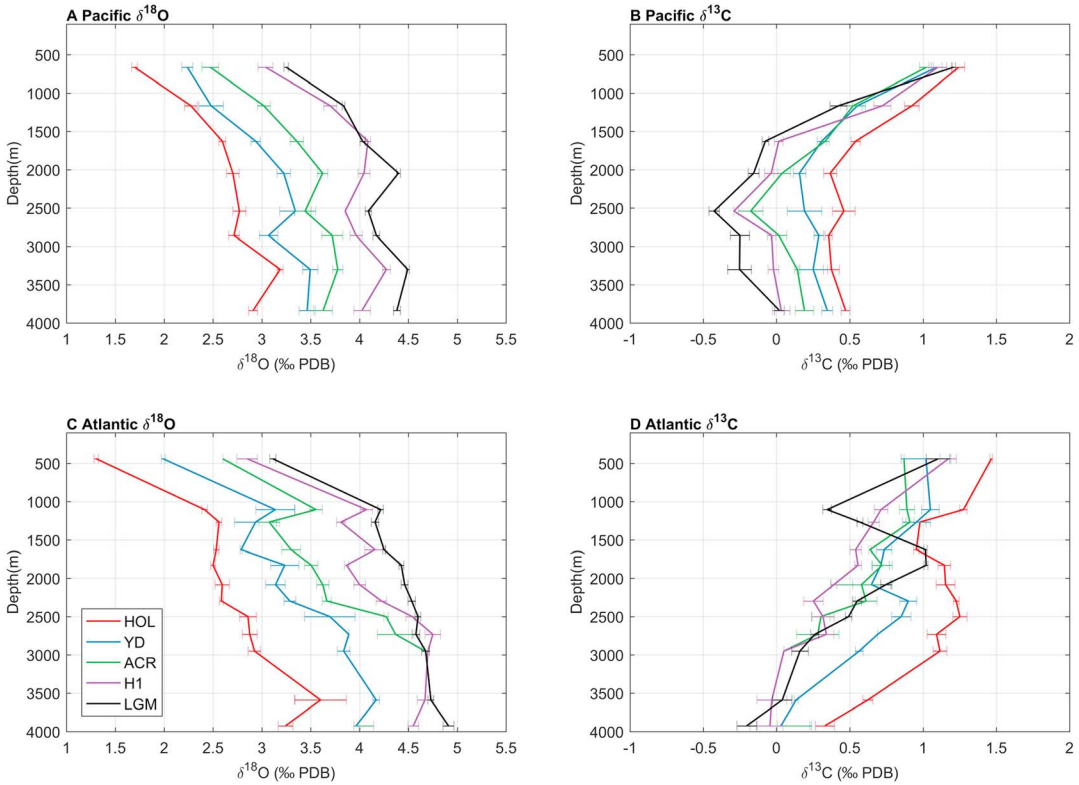

Figure 4. Benthic $\delta^{13}C$ and $\delta^{18}O$ profiles for each of the cores in the vertical transects. (a) Vertical profiles of averaged $\delta^{18}O$ for selected time slices in the Southwest Pacific: Glacial (19–23 ka), Heinrich Stadial 1 (HS1; 14.5.0–17.5 ka), Antarctic Cold Reversal (ACR; 12.9–14.5 ka), Younger Dryas (YD; 11–12.8 ka), and Holocene (Hol; 2.0–10.5 ka). (b) Vertical profiles of averaged $\delta^{18}O$ for selected time slices on the Brazil Margin. (c) Vertical profiles of average $\delta^{13}C$, using the same time slices and methods as Figure 4a. (d) Vertical profiles of average $\delta^{13}C$, using the same time slices and methods as Figure 4b. Horizontal bars display the errors of the means for each time slice and depth. Figure S5 provides an expanded version of this figure with the oceans overlaid for comparison. Figure S6 provides a collapsed version of this figure. Movies S1 and S2 provide video of the deglacial sequence of profiles available in the supporting information.

3. Results

3.1. Atlantic Versus Pacific $\delta^{18}O$

The LGM to Holocene isotopic transition across a broad depth profile in the individual basins has been previously described (Lund et al., 2015; Sikes, Elmore, et al., 2016). The focus of this paper is to observe Atlantic and Pacific differences during the LGM and last deglaciation. We examine the $\delta^{18}O$ differences between the two depth transects by comparing the $\delta^{18}O$ depth profiles through time and by calculating the differences between the basins ($\Delta\delta^{18}O$ = Atlantic $\delta^{18}O$ − Pacific $\delta^{18}O$), which were then contoured (Figure 3). Overall, $\Delta\delta^{18}O$ values were greater during the LGM, with the Atlantic at most depths being ~0.3‰ to 0.5‰ more enriched than the Pacific. The interbasin difference was greater below 2 km than above, with little to no difference at 2 km. During the deglaciation, there are several notable trends: $\Delta\delta^{18}O$ below 2.5 km increased to ~1‰ from the beginning of HS1 until the end of the YD, with the greatest difference in the 2.0 to 2.5 km depth range (Figure 3). After ~12 ka, $\Delta\delta^{18}O$ below 2.5 km diminished and transitioned from positive to negative in the late Holocene. The $\delta^{18}O$ difference at ~2 km remained close to 0 from the LGM, across the transition, and into the Holocene. At depths above 1.5 km, $\Delta\delta^{18}O$ was about ~0.3‰ from 23 to 3 ka, except for a brief increase to ~0.5‰ between 16 and 12 ka that was centered at depths above 1 km (Figure 3).

In order to determine the driver of the relative differences in $\delta^{18}O$ through time, it is necessary to examine the absolute $\delta^{18}O$ change in each basin. To examine these changes in relation to the millennial climate periods of the deglaciation, we averaged the $\delta^{18}O$ in each core for the LGM, HS1, ACR, YD, and the Holocene and plotted the results as depth profiles (Figure 4: also see supporting information Movies S1 and S2 for

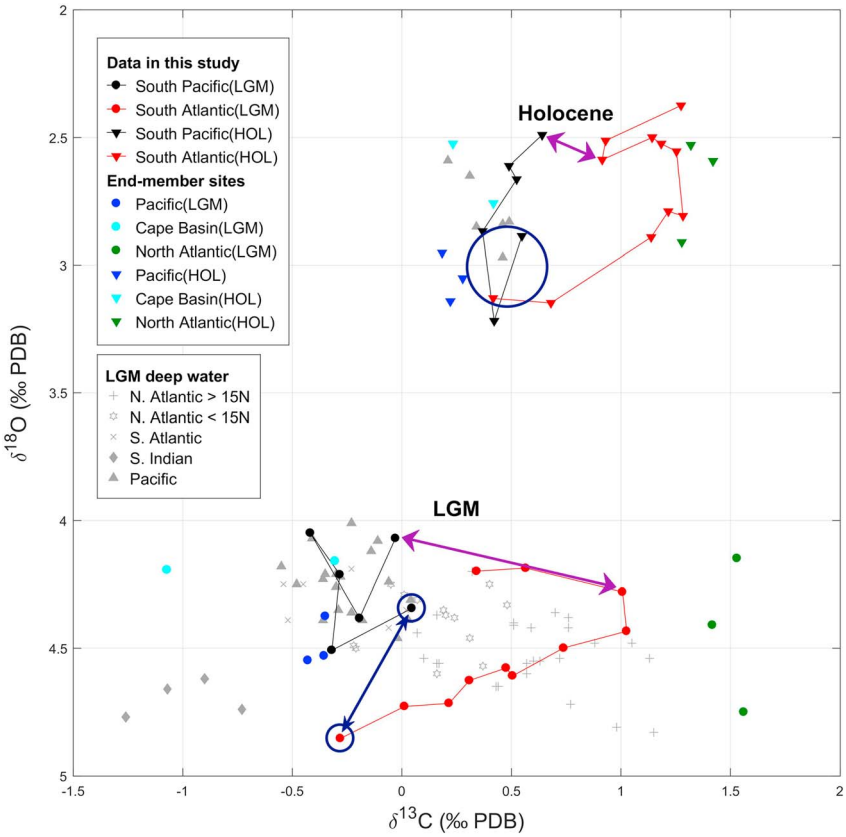

Figure 5. Cross plot of benthic $\delta^{18}O$ and $\delta^{13}C$ for the LGM and Holocene time slices. Data from this study for depths below 1 km are connected by lines in increasing depth order (Atlantic, red; Pacific black). Holocene, triangles; LGM circles. We do not include in this analysis the shallowest core from the Atlantic profile and the shallowest two cores from the Pacific. The purple arrows illustrate the contrast between the 1.1 km core in the Pacific profile with that of the 1.6 km core in the Atlantic profile for both time slices. The large blue circle encloses the values for the 3.8 km Pacific and 3.8 km Atlantic cores in the Holocene, whereas the small blue circles and blue arrow highlight the differences between those cores in the LGM. Cores representing end-members for the North Atlantic (green) and Pacific (blue) are plotted for both Holocene (triangles) and LGM (circles). Cape Basin cores are in turquoise. North Atlantic end-member cores are from ~1.2 to 1.6 km; these depths were chosen to correlate with the depth of GNAIW. They are NEAP 4 K (Rickaby & Elderfield, 2005), ODP984 (Praetorius et al., 2008), and RAPiD 10-1P (Thornalley et al., 2010). Pacific end-member cores are from 3.0 to 3.6 km: PS75/059-2 and PS75/056-1 (Ullermann et al., 2016); Cape Basin cores are from below 4.0 km: RC12-229 (Oppo & Fairbanks, 1987) and ODP-1089 (Hodell et al., 2003). The LGM core compilation represented by grey symbols designating their basins (as described in the figure legend), previously published by Duplessy et al. (2002) and Matsumoto and Lynch-Stieglitz (1999). With the exception of two cores from ~1.9 km cores all cores in this glacial compilation are from depths below 2 km. See Figure S7 for the location of Southern Hemisphere cores included in this figure.

animations of this figure). Higher deglacial $\Delta\delta^{18}O$ below 2 km appears to have been driven by changes in the Pacific; here $\delta^{18}O$ began to decrease at ~18 ka, while $\delta^{18}O$ in the deep Atlantic showed little change until the beginning of the Younger Dryas, about 5 kyr later (Figure 4). In contrast, above 1.5 km the $\delta^{18}O$ in both basins began to decrease early and continued to decrease throughout the deglaciation. At these shallower depths, the magnitude of change in the Pacific was small during HS1 (~0.2‰ or less), while the change in the Atlantic was variable but as large as ~0.5‰ (Figure 3). During the ACR, both basins experienced an ~1‰ depletion above 2.5 km and although the deep Pacific had a slightly smaller change, change in the Atlantic below 2.5 was negligible. During the YD, the Pacific had a depletion of ~0.5‰ across all depths, while change in the Atlantic was nearly 1‰ below 2.5 km. It is only after 6 ka, well into the Holocene, that the $\delta^{18}O$ profiles in both basins align (Figures 3 and 4). Sampling intervals in the upper portions of the deepest Atlantic cores are very coarse, so results for deepest depths after 16 ka are somewhat tentative.

3.2. Atlantic Versus Pacific $\delta^{13}C$

We examined the $\delta^{13}C$ differences ($\Delta\delta^{13}C$) between the two basins to infer relative changes related to exchange with the atmosphere, water mass mixing, and/or the accumulation of respired CO_2. The deep Pacific shows significantly greater ^{13}C depletion in waters below 1.5 km during the LGM than the Atlantic (with a maximum $\Delta\delta^{13}C$ of ~1.2‰ centered at ~1.8 km; Figure 3e). One of the most striking features of the LGM Atlantic was the well-characterized ^{13}C-enriched tongue centered at ~1.5 km (e.g., Curry & Oppo, 2005); (Figure 3d). This feature caused the Atlantic to be more enriched than the Pacific between 1.5 and 3.5 km throughout the LGM, deglaciation, and Holocene. There was a greater interbasin difference during the LGM (1 to 1.2‰) than the Holocene (~0.9‰; Figure 3e), and the interbasin difference was greatly diminished but did not disappear during the deglaciation. Throughout the LGM and the deglaciation, $\Delta\delta^{13}C$ at sites deeper than 3.5 km had neutral to slightly negative values, in strong contrast to the waters directly above. This interbasin homogeneity at depths between 3.6 and 4.1 km has been previously observed using cores from the East Pacific Rise and Cape Basins (Ullermann et al., 2016). At depths above 1.2 km during the LGM, the $\delta^{13}C$ in the Atlantic was slightly lower than the Pacific causing a small negative difference in $\Delta\delta^{13}C$ between the basins. This continued into the early deglaciation, until the ACR at about 14 ka. This appears to have been caused by a shallow pulse of enrichment in the Pacific above 1.6 km during the second half of HS1 that terminated in the ACR (Sikes, Elmore, et al., 2016). This difference diminished and became slightly positive from the ACR to the mid Holocene.

During the deglaciation, it is notable that $\delta^{13}C$ enrichment in the Pacific after HS1 occurred across all depths, while $\delta^{13}C$ changes in the Atlantic were variable and restricted to depths above 2.5 km until the YD (Figures 4 and S5). In the Atlantic during the HS1-YD interval, $\delta^{13}C$ from 1.5 to 3.5 km in the Atlantic was 0.1–0.5‰ lower than glacial values (Figure 3). The tongue of $\delta^{13}C$ enriched water that sat at ~1.5 km in the LGM subsequently deepened to be centered at 2.5 km and broadened, coincident with evidence of deepening of NADW in the Holocene (Gherardi et al., 2009). The reduction in $\Delta\delta^{13}C$ between 17 and 13 ka B.P. was driven by the large $\delta^{13}C$ decrease at middepths in the Atlantic. The ^{13}C changes in the respective basins are well resolved in the vertical profiles (Figure 4). The drop in $\Delta\delta^{13}C$ lasted for most of the deglaciation until approximately the YD, at which point the interbasin $\delta^{13}C$ difference strengthened followed by a deepening of the $\Delta\delta^{13}C$ maximum early in the Holocene.

4. Discussion

4.1. Atlantic Versus Pacific Water Mass Formation and Ventilation During the LGM

Although numerous studies have examined Atlantic-Pacific differences in $\delta^{13}C$ (Charles et al., 2010; Hodell et al., 2003; Ninnemann & Charles, 2002; Ullermann et al., 2016), few have examined $\delta^{18}O$ differences between the Atlantic and Pacific. The comparison of stacked $\delta^{18}O$ records has revealed the asynchronous arrival of deglacial signals among the ocean basins and across depths in the different basins (Stern & Lisiecki, 2014). Our comparison of depth transects reveals that throughout the past ~30 ka, Pacific and Atlantic $\delta^{18}O$ values at UCDW depths (centered at ~2 km) were much more similar than the $\delta^{18}O$ of water masses shallower and deeper in the water column. This suggests that the deeper and shallower water masses in the Pacific had significant inputs that were not directly sourced from AMOC flow out of the Atlantic. An important consideration in understanding this observation is that during the glaciation, northern sourced water likely shoaled to above ~2 km in the Atlantic (Curry & Oppo, 2005; Gherardi et al., 2009; Lund et al., 2015). The prevailing assumption has been that waters from this shallow AMOC flow still entered the Southern Ocean, similar to today, an assumption we suggest deserves revisiting.

To explain the Atlantic-Pacific differences in $\delta^{18}O$ during the LGM, we make the argument that unlike today, PDW was the dominant source of water below 2 km, largely replacing NADW as the main contributor. This suggestion derives from the understanding that dynamically, waters entering the Southern Ocean above the sill depth of the Drake Passage cannot cross the ACC (see review in Talley, 2013, and Toggweiler & Samuels, 1995). In contrast, waters below this depth are able to flow southward in geostrophic balance, due to the east-west pressure gradient created by Drake Passage. Today, the core of the NADW enters the Southern Ocean below this sill depth (approximately 2.5 km) and upwells to the sea surface in the regions south of the ACC, making it the main input for dense water formation processes in the Ross and Weddell

Seas that yield AABW (e.g., Warren, 1990) (Figure 2a). These dynamical constraints require that the shoaling of NADW during the LGM to depths above 2 km would have prevented these waters from entering the deep Southern Ocean. Similar to waters above the Drake Passage sill depth today, they would have been restricted to locations north of the ACC where the shallow water masses SAMW and AAIW form (Talley, 2013).

If NADW was not a primary source of abyssal Southern Ocean waters during the LGM, then what was? We suggest that the roles of NADW and PDW were reversed during the LGM. Today, the less dense PDW and IDW outcrop north of the NADW in the Southern Ocean and are the dominant source for the northward flow of surface waters subducted into SAMW and AAIW (Marshall & Speer, 2012; Talley, 2013) (Figure 2a). It is these water masses, rather than NADW, that provide nutrients delivered to thermocline waters at lower latitudes (Sarmiento et al., 2004; Talley, 2013). With GNAIW being demonstrably shallower and presumably less dense than IDW/PDW during glacial times, we suggest that IDW/PDW outcropped south of GNAIW and supplied the waters that flowed southward to eventually form LCDW and AABW (Figure 2b). We lay out the evidence that supports our proposed mechanism below.

In the upper portion of the water column in our two transects, the glacial isotopic differences can be explained by the shoaling of North Atlantic sourced waters to depths above 2 km (Curry & Oppo, 2005). Our mechanism predicts that these waters were restricted to the north of the ACC, making them a dominant source for glacial SAMW and AAIW, primarily in the Atlantic. Today, water upwelled north of the core of the ACC in the Indian Ocean freshens and warms to form SAMW and AAIW as it transits to the Pacific. But during the LGM, northward movement of the STF would have largely restricted the influence of northern sourced waters to the Atlantic basin (Beal et al., 2011; Peeters et al., 2004). This suggests that intermediate waters in the Atlantic were sourced from GNAIW, whereas Indian and Pacific intermediate waters were primarily sourced from PDW/IDW (Figure 2b). The main result was that interconnectedness of the major ocean basins observed today through the intertwining of the conveyor belt in the modern configuration was reduced to exchange above the sill depth of Drake Passage (Figure 2b). This mechanism is similar to that of Ferrari et al. (2014), but instead of calling solely on expanded Southern Ocean sea ice to create two distinct deep circulation cells, we invoke a key role for the Drake Passage gateway as well. We suggest that this would not only isolate deep waters from shallower interior water masses in the Atlantic; it would also create separate deep circulation cells in the Atlantic and Pacific basins.

4.1.1. The Glacial Deep Ocean

The largest Atlantic-Pacific $\delta^{18}O$ differences were observed below ~2.5 km from the LGM into the early Holocene. The positive $\Delta\delta^{18}O$ signal suggests that the deep South Atlantic was colder and/or saltier than the deep Pacific (Figures 3c and S5). Lacking the input of dense NADW across the ACC, abyssal waters that formed in the Southern Ocean (AABW) would not have been "just recycled NADW" as they are today (Warren, 1990). Modification of the $\delta^{18}O$ signature as CDW flows from the Atlantic to Pacific has a negligible effect on the surface $\delta^{18}O$ signal today (LeGrande & Schmidt, 2006). Alteration along this path in the LGM that depleted the $\delta^{18}O$ through deep water formation processes was unlikely. Brine rejection during the formation of sea ice increases salinity and only weakly depletes the oxygen isotopes of the remaining water (Craig & Gordon, 1965). Cooling through open ocean convection processes (polynya formation) would enrich the $\delta^{18}O$ of calcite formed relative to the source waters, pushing the interbasinal signal in the wrong direction. Although precipitation would tend to deplete the signature (LeGrande & Schmidt, 2006), any freshwater input would decrease density contributing more to shallow water formation. Although the cooling of water beneath ice shelves would produce a negative $\delta^{18}O$ signature reflecting incorporation of overlying ice shelf meltwater, this formation mechanism is controlled by the position of the grounded ice sheet relative to the continental shelf break and can be largely disallowed during the LGM because continental glaciers reached to the continual shelf edge (e.g., Anderson et al., 2014; Hillenbrand et al., 2013). Instead, the relatively depleted $\delta^{18}O$ of deep Pacific waters can be attributed to the diffusively formed nature of IDW/PDW that is derived mostly from upwelled AABW admixed with low-latitude sourced waters (with depleted $\delta^{18}O$) within the midlatitudes of the Indian and Pacific Oceans. These processes move the deep waters upward and to lower density even though the diffusive processes are weak (Talley, 2013). We infer that IDW/PDW densities were greater than GNAIW causing the roles of IDW/PDW and North Atlantic source waters to be reversed. GNAIW, which was unable to cross the ACC, if it contributed to deep water formation at all, likely had its influence restricted to the Atlantic basin. Consequently, we argue that the independent nature of these pathways in forming southern sourced interior waters was greater during the LGM than today and

that Pacific and Indian water masses became important sources forming both shallower and deeper water masses in the Pacific during the LGM and early deglaciation.

There is evidence for reduced flow through Drake Passage in the LGM (Lamy et al., 2015; McCave et al., 2014), which supports our hypothesis of reduced communication between the Southern Ocean basins. Notably, 2.5 km is the sill depth of not only the Drake Passage but also about the depth of ridges separating the deep the Indian Ocean from the Pacific in the Southern Ocean (Figure 1). Enhanced stratification observed in the South Atlantic (Roberts et al., 2015) could have caused these sills to isolate abyssal waters originating in the Weddell and Ross Sea regions (McCave et al., 2008) and would have restricted mixing of the deepest waters. Other lines of geochemical evidence confirm that deepest waters in the South Atlantic sector of the Southern Ocean were saltier than the Southern Pacific (Adkins et al., 2002) and were about the same temperature (Elderfield et al., 2010; Roberts et al., 2015). Relatively fresh waters in the deep Pacific compared to the South Atlantic are consistent with the idea that they originated from different sources and/or were influenced by mixing with different water masses. In this situation, bottom and deep waters formed in the Weddell Sea were sourced from the reduced UCDW inflow through Drake Passage interacting with AABW present in that basin, whereas deep waters in the Pacific would have been derived from IDW/PDW with different water mass characteristics. This scenario is supported by the difference in the Atlantic-Pacific $\delta^{13}C$ in our profiles, with the Atlantic at depths between ~1.5 and 2.8 km significantly more $\delta^{13}C$ enriched/ventilated than the Pacific (Figure 3). Notably, this $\delta^{13}C$ divide in the Atlantic shoaled to sill depth at the latitude of Drake Passage (~2.5 km) (Curry & Oppo, 2005). Many lines of evidence, including $\Delta^{14}C$, have suggested that the ocean's geochemical divide shoaled in the LGM (e.g., Curry & Oppo, 2005; Ferrari et al., 2014; Sikes, Cook, et al., 2016, Sikes, Elmore, et al., 2016). Modeling results indicate that reduced bottom drag, consistent with a weaker ACC, leads to shallower stratification with the volume of circumpolar transport relatively insensitive to surface wind stress (Marshall et al., 2017). Based on this, we infer that the glacial increase in stratification may have been linked to the inferred reduction in ACC flow. Our basinal comparison supports this mechanism and adds an important third dimension to previous two-dimensional conceptualizations of global overturning circulation (Figure 2). A greater independence of deep water formation and recirculation in the Pacific during the LGM and the restriction of North Atlantic source waters from the Southern Ocean would have enhanced the role of IDW/PDW in deep water formation, resulting in greater isolation of deep water masses in the Pacific in the LGM.

We can examine the differences between the deeper portions of our profiles during the LGM and Holocene by cross plotting the $\delta^{13}C$ and $\delta^{18}O$ in our profiles, disregarding data from above 1 km (the shallowest core from the Atlantic profile and the shallowest two cores from the Pacific; Figure 5). This allows us to focus on the composition of deep internal water masses. During the Holocene, the data from our Atlantic and Pacific depth transects plot close together in $\delta^{13}C$ and $\delta^{18}O$ space (red and black symbols in Figure 5). In particular, the deepest points where the $\delta^{13}C$ values in each profile converge point to a common source of abyssal waters in the two basins (highlighted by the large, open black circle in Figure 5). In contrast, during the LGM the largest difference between our Pacific and Atlantic profiles is in $\delta^{13}C$ at ~1.5 km, which indicates a greater buildup of respired carbon in the Pacific, which we infer as reduced exchange between the basins. During the LGM, the $\delta^{18}O$ contrast between the deep basins is represented by the vertical distance between cores at similar depths on this plot (highlighted by the arrows in Figure 5). The larger $\delta^{18}O$ difference at 4 km between the South Pacific and South Atlantic profiles during the LGM signals the greater geochemical separation of these basins (indicated by the open black circles in Figure 5).

We can further assess the differences between the deeper portions of the basins during the LGM and Holocene by comparing the $\delta^{13}C$ and $\delta^{18}O$ in our profiles to hypothetical end-members from the eastern Pacific and the North Atlantic (Figure 5). Note that the overall spread in deep ocean $\delta^{13}C$ data between North Atlantic and Pacific end-members is approximately 1.2‰ during the Holocene (blue and dark green symbols in Figure 5). In contrast, the spread in deep ocean $\delta^{13}C$ end-members during the LGM was approximately 2.5‰, suggesting a greater buildup of respired carbon in Southern Ocean and Pacific basins, apparently enhanced by reduced exchange between deep basins. Larger differences between Pacific and Atlantic deep water compositions in $\delta^{18}O$- $\delta^{13}C$ space are a widespread feature and have been observed at a number of abyssal depth cores from the Atlantic, Pacific, and Southern Oceans (Duplessy et al., 2002; Matsumoto & Lynch-Stieglitz, 1999) (Figure 5).

The differences in the $\delta^{13}C$ signatures between the Holocene and LGM also have some interesting nuance. In the Holocene, the $\delta^{13}C$ values in our profiles sit between the end-member values (which are from similar depths) and are closely bounded by them, with the difference between our profiles and the respective $\delta^{13}C$ end-members separated by about 0.2‰ in both oceans. During the LGM, not only was the difference between end-members larger, the composition of deep waters globally tended to shift toward Pacific values. Specifically, the values in our Atlantic profile from 1.5 to 2.5 km were at least 0.5‰ more depleted in $\delta^{13}C$ relative to the North Atlantic end-member cores from the same depths, whereas the Pacific end-member sites cluster with our Pacific profile (Figure 5). The shift of the South Atlantic $\delta^{13}C$ profile farther away from the North Atlantic end-member is accompanied by an increase in the contrast between the shallower and deeper cores in our Brazil Margin profile. Although this implies a greater buildup of CO_2 as water transited through Atlantic during the LGM than today, this was limited to depths below 3 km which has also been attributed to mixing of end-members (Hoffman & Lund, 2012). In contrast, the Pacific end-members (blue circles, Figure 5) had the same values as our South Pacific profile, all depths had similar $\delta^{13}C$ values, and these cluster with numerous sites in the North and equatorial Pacific (Duplessy et al., 2002) (Figure 5). Conspicuously, the Pacific sites also cluster with South Atlantic sites below 3.5 km (Figure 5). The similarity in the $\delta^{13}C$ of the two basins has been noted in previous comparisons of cores from between 3 and 4 km (Charles et al., 2010; Hodell et al., 2003; Ninnemann & Charles, 2002; Ullermann et al., 2016). We suggest that this is evidence that the Pacific sector of the Southern Ocean *was* the end-member for much of the global ocean during the LGM, and we speculate that a significant amount of this deep water was forming in the Ross Sea with PDW as a dominant source. A limited connection to the abyssal Atlantic through Drake Passage at 2–2.5 km and the lack of a significant contribution from the North Atlantic to the Pacific and Indian basins could explain these observations.

It is important to note that there are five cores that do not fall within the Atlantic-Pacific continuum (Figure 5). These sites, which are distinguished by their extremely depleted $\delta^{13}C$ values (Hodell et al., 2003; Ullermann et al., 2016), are from the southwest Indian Ocean sector below 3.0 km and the Cape Basin below 4 km in the Southeast Atlantic (grey diamonds and turquoise circles, Figures 5 and S7). All five of the sites are below the sill depth that separates the deepest Southern Atlantic from the western Indian Ocean basin (~3.2 km) and the Indian from the Pacific (~2.5 km; Figure 1). The deepest core in our Atlantic transect has similarly enriched $\delta^{18}O$ and $\delta^{13}C$ approaching these values. Based on the unique $\delta^{13}C$ signature and spatial isolation of the five sites, we speculate that the deepest waters in this region formed in the Weddell Sea and were largely restricted to the southwest Indian Ocean and Southeast Atlantic during the LGM, whereas Pacific AABW formed in the Ross Sea as first suggested by McCave et al. (2008) with a different source pathway and ventilation history.

4.1.2. Shallow Layers of the Southern Ocean

At midwater depths of around 2 km, located above the sills in the Southern Ocean, the Pacific and Atlantic $\delta^{18}O$ values were more similar to each other than waters above and below from the LGM through the early Holocene. This suggests that waters at UCDW depths were swept westward in the ACC flow, moving around Antarctica with little modification of their $\delta^{18}O$, similar to today. At depths above 1.5 km, the observed positive Atlantic-Pacific $\Delta\delta^{18}O$ during the LGM implies that waters in the Pacific were fresher and/or warmer. This suggests that there were similar formation processes as today in the Indian and Southwest Pacific sector that freshen intermediate waters as they move eastward (McCartney, 1977).

Notably, the most positive $\Delta^{13}C$ values for any given time interval occurred during the LGM and were located between 1.5 and 2.5 km water depths. This significant fact, that North Atlantic sourced waters at middepths were continuously more ^{13}C enriched than the Pacific, suggests the uninterrupted accumulation of respired CO_2 along a shoaled AMOC-style conveyor circulation throughout the LGM, deglaciation, and Holocene (Lund et al., 2011; Lynch-Stieglitz et al., 2007). This is compelling evidence against any "reversal" in water mass circulation patterns during the LGM, with the implication that North Pacific Deep Water formation, if it occurred, was not vigorous enough to have a demonstrable effect on interbasin $\delta^{13}C$ gradients.

Water at SAMW/AAIW depths above 1.0 km in the Pacific was more enriched in $\delta^{13}C$ during the LGM than the Atlantic. Significantly, although the interbasin $\Delta\delta^{13}C$ signal was negative during the LGM, there was no $\delta^{18}O$ enrichment (Figure 3). In the Pacific, intermediate $\delta^{13}C$ is predominantly set by exchange with the atmosphere (Lynch-Stieglitz et al., 1994) and any $\delta^{13}C$ enrichment due to LGM cooling would require an attendant drop in $\delta^{18}O$ which is not observed. A reduced contribution from intermediate depth Atlantic Ocean waters

in favor of contributions from upwelled IDW/PDW (Lynch-Stieglitz et al., 1994) and enhanced air-sea exchange of CO_2 can explain these observations.

Overall, our results show that the glacial ocean was not simply composed of a deep and shallow cell with similar chemical compositions across basins. Pacific and Atlantic $\delta^{13}C$ and $\delta^{18}O$ offsets were generally greater during the LGM than they are today. This is an important distinction that refines the mechanism for observed differences between upper and lower cells during glacial times (Hu et al., 2016; Sikes, Elmore, et al., 2016; Stern & Lisiecki, 2014) by imposing a horizontal separation as well.

4.2. Atlantic Versus Pacific Water Mass Structure During the Deglaciation

The deglacial changes in the two basins can be summarized as follows. The Pacific experienced early shifts in both $\delta^{18}O$ and $\delta^{13}C$; these changes were relatively (though not completely) uniform across all depths, and this transformation progressed relatively steadily throughout HS1, the ACR, and the YD. In contrast, the primary $\delta^{18}O$ and $\delta^{13}C$ changes in the Atlantic occurred above 2.5 km throughout HS1 and the ACR, and only after the ACR did waters below 2.5 km show a clear shift toward Holocene values. These contrasting behaviors are best illustrated by the differences between the vertical depth profile time slices for each ocean (Figure 4; see the supporting information Movies S1 and S2 and Figures S5 and S6). The changes in the South Atlantic can largely be characterized as the response to deglacial changes in AMOC and the end-member composition of northern component water (Lund et al., 2015; McManus et al., 2004; Oppo et al., 2015; Tessin & Lund, 2013). The lack of isotopic change in the deep Atlantic until the ACR or later fits with other lines of evidence that AMOC flow did not deepen to below 2.5 km, the Drake Passage sill depth, until after the YD (Gherardi et al., 2009). The shallow AMOC flow that persisted through the early deglaciation would have precluded AMOC flow from crossing the ACC and entering the deep Southern Ocean. We argue that this situation requires that deglacial water mass changes in the Pacific, particularly the early $\delta^{13}C$ enrichment at shallow depth and shifts in $\delta^{18}O$ and $\delta^{13}C$ in deeper waters, must have had an independent driver from the Atlantic. We provide details of the deglacial progression in both basins within the framework of millennial-scale climate and circulation changes that support a deep gateway as a possible controlling mechanism below.

4.2.1. Heinrich Stadial 1

The earliest stages of the deglaciation during Heinrich Stadial 1 brought a stable isotope response in the Atlantic that was largely restricted to water depths above 2.5 km. The LGM to HS1 reduction of ~0.5‰ in $\delta^{18}O$ was most likely due to the delivery of a meltwater signal at middepths (Lund et al., 2015) because waters at these depths in the South Atlantic did not warm appreciably until the ACR (Lund et al., 2015; Roberts et al., 2015). The depletion in $\delta^{13}C$ has been attributed to reduced AMOC flow associated with HS1 and the accumulation of respired carbon at middepths (Gherardi et al., 2009; McManus et al., 2004; Schmittner & Lund, 2015). In the Pacific, $\delta^{13}C$ had the opposite signal with depths shallower than 1.5 km becoming more enriched during the second half of HS1 (Figures 3 and S6). This intermediate depth $\delta^{13}C$ enrichment cannot be explained by temperature because existing Mg/Ca records show contemporaneous warming near AAIW formation zones (Hertzberg et al., 2016). Instead, $\delta^{13}C$ enrichment in the Pacific has been attributed to two mechanisms: (1) decreased efficiency of the biologic pump (Jaccard et al., 2016; Schmittner & Lund, 2015) which could occur before the net flux of CO_2 to the atmosphere or (2) wind-driven exchange caused by the southward shift in Southern Westerlies (Anderson et al., 2009; Putnam et al., 2013) that enhanced shallow ventilation in the Pacific (Sikes, Elmore, et al., 2016) which should occur simultaneously or lag somewhat the atmosphere CO_2 increase. Either mechanism is consistent with net flux of carbon from the ocean to the atmosphere and the overall increase in atmospheric CO_2 in the latter part of HS1 (Marcott et al., 2014). Mechanism 2 supports the view that the pulse of atmospheric CO_2 at 16.5 ka (Marcott et al., 2014) came largely from intermediate waters in the Pacific (Sarnthein et al., 2013; Sikes, Cook, et al., 2016, Sikes, Elmore, et al., 2016).

In the Pacific, there was a $\delta^{18}O$ depletion of ~0.3‰ throughout the water column below 2.0 km (Figure 3). The $\delta^{18}O$ change must have been largely due to freshening because deep water temperatures in this region of the Pacific did not warm until ~15 ka (Elderfield et al., 2012). The deep Pacific change was smaller than that observed in the upper Atlantic and occurred in advance of any deep changes in the Atlantic (Figures 4 and S5). If AMOC flow was diminished in HS1 (McManus et al., 2004), this may have lessened northern source waters' influence on waters in the Southern Ocean. The consistent $\delta^{18}O$ shifts

across all depths in the Pacific indicate early modifications in middle to deep water formation. The possibility that a meltwater signal was transported laterally in the ACC and subsequently incorporated in the formation of deeper waters in the Pacific cannot be dismissed, but if meltwater influenced the deep Pacific, why did it not affect the deep Atlantic until the YD? Alternatively, we attribute the Pacific signal to reductions in Southern Ocean sea ice extent (Wolff et al., 2006) and shifts in wind location (Denton et al., 2010) that enhanced upwelling (Anderson et al., 2009) as a means to invigorate deep water formation and suggest that these dynamic changes altered the composition of waters formed in the Southern Ocean.

We note here that we were surprised to find that the relative timing of these early $\delta^{18}O$ changes between basins in our depth transects are different from those seen in stacked records comparing the onset of the glacial termination between basins (Stern & Lisiecki, 2014). Stacked records indicate that the deep South Atlantic led the deep Pacific. We are uncertain of the reason for the differences in the records but suggest that the stacking process which combined cores from 2 to 4 km depth and across the entire Pacific for comparison may have masked some of the detail we see in our depth transects.

4.2.2. The Antarctic Cold Reversal

During the ACR, Atlantic $\delta^{18}O$ declined by 0.5–1.0‰ at depths above 2.5 km, which could be attributed to the delivery of meltwater and warming of shallow water masses (Lund et al., 2015; Roberts et al., 2015). This was accompanied by $\delta^{13}C$ enrichment, perhaps attributable to reinvigoration of shallow AMOC in the Bølling-Allerød interval (Gherardi et al., 2009; Lund et al., 2015). At the same time, benthic $\delta^{18}O$ in the Pacific above 2.5 km experienced a reduction similar to the Atlantic (Figures 3 and 4). By the ACR the STF had moved sufficiently southward of Africa (Beal et al., 2011; Peeters et al., 2004), to have allowed eastward transport in shallow waters north of the ACC. The large decrease in $\delta^{18}O$ at ~1500 m in the Pacific suggests the renewed transport of a $\delta^{18}O$-depleted meltwater signal to Pacific intermediate water masses during the ACR (Figure 4). For water masses above 2000 m, relatively fresh intermediate waters sourced from the North Pacific may have exerted some influence as well (Cook et al., 2016).

While there were no large changes in either $\delta^{13}C$ or $\delta^{18}O$ in the deep Atlantic during the ACR, the deep Pacific continued to migrate toward Holocene values. Deepening $\delta^{13}C$ enrichment in the Pacific of greater magnitude than the Atlantic reduced the deep interbasin $\delta^{13}C$ gradient until it reached a minimum at ~13 ka, near the end of the ACR (Figure 3). Throughout this interval, $\delta^{13}C$ enrichment in the Pacific at depths below 3 km led the Atlantic, which suggests continued and deepening ventilation in the Pacific from HS1 to the ACR. The resolution of the deep South Atlantic stable isotope data is poor through the ACR, but $\Delta^{14}C$ evidence from multiple locations suggests that enhanced ventilation in the upper Atlantic occurred at the onset of the ACR (Burke & Robinson, 2012; Chen et al., 2015; Skinner et al., 2015). At the same time, the lack of change in the deep Atlantic $\delta^{18}O$ caused the deep basins' $\delta^{18}O$ to be most dissimilar from HS1 to the end of the ACR (Figures 3 and 4). This is supported by benthic stacks for deep waters in these regions (Stern & Lisiecki, 2014). Evidence suggests that AMOC remained shoaled in the Atlantic during the ACR (Gherardi et al., 2009). From this we infer that while frontal movement southward may have reinitiated communication between the basins at intermediate depths, communication below the Drake Passage sill depth continued to be restricted, causing the chemistry of the deeper waters to remain distinct owing to circulation constraints rather than stratification. The rapid change in Atlantic carbon isotopes compared to the sluggish change in the Pacific suggests that the rapid rise in atmospheric CO_2 at 14.6 ka (Marcott et al., 2014) came largely from the deep Atlantic, with little participation from the Pacific.

4.2.3. The YD Into the Holocene

It was not until the YD that the deep Atlantic carbon and oxygen isotopes approached Holocene values and structure. The resolution in our deep Atlantic cores is low for this period, but this behavior is confirmed in other records (Roberts et al., 2015). During the YD, the Pacific above 2.5 km experienced greater reductions in $\delta^{18}O$ than the Atlantic (~0.6‰). This requires that any $\delta^{18}O$-depleted meltwater signal transported in shallow waters north of the ACC was also augmented by Southern Ocean processes such as warming and/or freshening that further modified Pacific intermediate water masses, similar to today. The interbasinal $\Delta\delta^{13}C$ that was greatly reduced in the early deglaciation relative to the LGM began to increase, broaden, and deepen into the Holocene, coincident with evidence of deepening of NADW in the Holocene (Gherardi et al., 2009), indicating the resumption of the interbasinal flow seen today. The cessation of meltwater input to the North Atlantic would have allowed AMOC flow to become more salty (Roberts

et al., 2015), and this could have driven the onset of modern-style deeper NADW transport that allowed the escape of NADW into the Southern Ocean by the early Holocene (Figures 3 and 4). These changes in deep circulation and carbon storage appear to have completed the shift of the system into an interglacial mode.

5. Summary and Conclusions

Pacific and Atlantic benthic $\delta^{13}C$ and $\delta^{18}O$ isotope depth profiles during the LGM were distinct from one another and from their respective Holocene profiles. This interbasinal dissimilarity is an important feature that suggests different circulation cells in the two oceans. This circulation feature is in addition to changes brought about by AMOC shoaling that is suggested to have partitioned the glacial ocean into relatively isolated upper and lower cells (Ferrari et al., 2014). Geostrophic balance requires that the glacial shoaling of AMOC flow would have prevented GNAIW from entering the eastward flow of the ACC. With the northward migration of Southern Ocean fronts south of Africa, flow north of the ACC into the Indian Ocean would have been largely reduced (Beal et al., 2011; Peeters et al., 2004). From this we deduce that GNAIW would not have entered the Southern Ocean and must have been restricted to the Atlantic providing a source for shallow interior water masses such as SAMW and AAIW, which we conjecture were mainly restricted to the Atlantic. In this extreme case, IDW and PDW would have continued to be the main source for Pacific and Indian SAMW and AAIW, in addition to becoming the primary source of dense waters in the Pacific basins where AABW formed (Figure 2b). This altered glacial circulation would have driven deep circulation in the two oceans to be more independent in the LGM as evidenced by the contrasting isotopic profiles in the two basins (Figures 3 and 4). Our end-member analysis suggests that recirculation in the Pacific driven by Southern Ocean processes appears to have supplied most of the ventilation for that basin in the LGM.

The structure of the vertical profiles of $\delta^{18}O$ in the two basins was increasingly dissimilar through the deglaciation, with our $\delta^{18}O$ results showing changes in Pacific sector Southern Ocean deep water character that began earlier than changes in the Atlantic and well before AMOC circulation deepened and/or strengthened. This suggests a density structure that was not only dissimilar between the basins but also that any physical destratification may have proceeded at different times in the two oceans. Change occurred rapidly after the YD as AMOC deepened, opening a deep gateway to reconnect the Atlantic with Southern Ocean basins in the Indian and Pacific. A decrease in the density of deep water has been invoked to explain the deglacial rise in atmospheric pCO_2, via changes in the rate of diapycnal mixing and the vertical position of the isopycnal separating the two overturning branches of circulation (Ferrari et al., 2014). We suggest that the depth to which northern sourced waters sank was a critical governor on their ability to participate in Southern Ocean processes. Southern Ocean processes in the Pacific may have been more important in regulating initial degassing of CO_2 to the atmosphere through most of the deglaciation until this deep pathway reopened.

Our comparison of $\delta^{13}C$ profiles and the pace of isotopic change at different depths leads us to suggest that the initial atmospheric CO_2 rise from 17.5 to 16 ka ventilation came from the shallow Pacific driven by upwelling processes (Anderson et al., 2009; Sikes, Elmore, et al., 2016) that were independent of AMOC-driven change in the South Atlantic. Based on $\delta^{13}C$ enrichment, the deeper layers of the Pacific appear to have contributed CO_2 steadily and from increasingly deeper depths throughout the deglaciation. The deep Atlantic appears to have contributed only after the ACR when AMOC deepened to become NADW and again contributed to deep water formation and ventilation in the Southern Ocean.

Acknowledgments
Discussions at the PAGES-sponsored IPODS/OC3 workshop in Bern, 2013, initiated the work in this paper, and all the authors wish to acknowledge travel support from PAGES that fostered the work presented here. We wholeheartedly thank Eli Hunter who produced all the figures and conducted the numerical analyses that went into them. Our great appreciation goes to John Wilkin for numerous discussions clarifying Southern Ocean physics on which the interpretations stand. Funding for this project came from NSF OCE-0823487 and 0823549-03 to E. L. S. and NSF OCE-1003500 to D. C. L. This work was also cultivated by fellowships from the Hanse-Wissenschaftskolleg to E. L. S. and K. A. A. Support was also provided by the NOAA Climate and Global Change Program to K. A. A., administered by the University Corporation for Atmospheric Research. All data used in this paper were archived under the original publication citations (Lund et al., 2015; Sikes, Elmore, et al., 2016) with the NOAA Centers for Environmental Information in the online paleoclimate database: http://www.ncdc.noaa.gov/data-access/paleoclimatology-data.

References

Adkins, J. F. (2013). The role of deep ocean circulation in setting glacial climates. *Paleoceanography*, *28*, 539–561. https://doi.org/10.1002/palo.20046

Adkins, J. F., McIntyre, K., & Schrag, D. P. (2002). The salinity, temperature, and ^{18}O of the glacial deep ocean. *Science*, *298*, 1769–1773.

Allen, K. A., Sikes, E. L., Hönisch, B., Elmore, A. C., Guilderson, T. P., Rosenthal, Y., & Anderson, R. F. (2015). Southwest Pacific deep water carbonate chemistry linked to high southern latitude climate and atmospheric CO_2 during the Last Glacial Termination. *Quaternary Science Reviews*, *122*, 180–191.

Anderson, J. B., Conway, H., Bart, P. J., Witus, A. E., Greenwood, S. L., McKay, R. M., … Stone, J. O. (2014). Ross Sea paleo-ice sheet drainage and deglacial history during and since the LGM. *Quaternary Science Reviews*, *100*, 31–54.

Anderson, R. F., Ali, S., Bradtmiller, L. I., Nielson, S. H. H., Fleisher, M. Q., Anderson, B. E., & Burckle, L. H. (2009). Wind-driven upwelling in the Southern Ocean and the deglacial rise in atmospheric CO_2. *Science*, *323*, 1441–1448.

Angulo, R. J., Souza, M. C. D., Reimer, P. J., & Sasaoka, S. K. (2005). Reservoir effect of the southern and southeastern Brazilian coast. *Radiocarbon*, *47*(1), 67–73.

Balmer, S., Sarnthein, M., Mudelsee, M., & Grootes, P. M. (2016). Refined modeling and ^{14}C plateau tuning reveal consistent patterns of glacial and deglacial ^{14}C reservoir ages of surface waters in low-latitude Atlantic. *Paleoceanography*, *31*, 1030–1040. https://doi.org/10.1002/2016PA002953

Beal, L. M., De Ruijter, W., Biastoch, A., Zahn, R., & SCOR/WCRP/IAPSO Working Group 136 (2011). On the role of the Agulhas system in ocean circulation and climate. *Nature*, *472*(7344), 429–436.

Belkin, I. M., & Gordon, A. L. (1996). Southern Ocean fronts from the Greenwich meridian to Tasmania. *Journal of Geophysical Research*, *101*, 3675–3696. https://doi.org/10.1029/95JC02750

Bostock, H. C., Opdyke, B. N., & Williams, M. J. M. (2010). Characterizing the intermediate depth waters of the Pacific Ocean using $\delta^{13}C$ and other geochemical tracers. *Deep Sea Research, Part I*, *57*, 847–859.

Boyle, E. A. (1988). Vertical ocean nutrient fractionation and glacial/interglacial CO_2 cycles. *Nature*, *331*, 55–56.

Boyle, E. A., & Keigwin, L. D. (1987). North Atlantic thermohaline circulation during the past 20,000 years linked to high-latitude surface temperature. *Nature*, *330*, 35–40.

Burke, A., & Robinson, L. F. (2012). The Southern Ocean's role in carbon exchange during the last deglaciation. *Science*, *335*, 557–561.

Charles, C. D., & Fairbanks, R. G. (1992). Evidence from Southern Ocean sediments for the effect of North Atlantic deep-water flux on climate. *Nature*, *355*, 416–419.

Charles, C. D., Pahnke, K., Zahn, R., Mortyn, P. G., Ninnemann, U., & Hodell, D. A. (2010). Millennial scale evolution of the Southern Ocean chemical divide. *Quaternary Science Reviews*, *29*, 399–409.

Charles, C. D., Wright, J. D., & Fairbanks, R. G. (1993). Thermodynamic influences on the marine carbon isotope record. *Paleoceanography*, *8*, 691–697. https://doi.org/10.1029/93PA01803

Chen, T., Robinson, L. F., Burke, A., Southon, J., Spooner, P., Morris, P. J., & Ng, H. C. (2015). Synchronous centennial abrupt events in the ocean and atmosphere during the last deglaciation. *Science*, *349-1541*(6225), 1537–1541.

Chiswell, S. M., Bostock, H. C., Sutton, P. J. H., & Williams, M. J. M. (2015). Physical oceanography of the deep seas around New Zealand: A review. *New Zealand Journal of Marine and Freshwater Research*, *49*, 286–317.

Cook, M. S., Ravelo, A. C., Mix, A., Nesbitt, I. M., & Miller, N. V. (2016). Tracing subarctic Pacific water masses with benthic foraminiferal stable isotopes during the LGM and late Pleistocene. *Deep Sea Research, Part II*, *125-126*, 84–95.

Craig, H., & Gordon, L. I. (1965). Deuterium and oxygen 18 variations in the ocean and the marine atmosphere. In E. Tongiorgi (Ed.), *Stable isotopes in oceanographic studies and paleotemperatures* (pp. 9–130). Spoleto, Italy: Cons. Naz. di Rech.

Curry, W. B., Duplessy, J.-C., Labeyrie, L. D., & Shackleton, N. J. (1988). Changes in the distribution of $\delta^{13}C$ of deep water ΣCO_2 between the last glaciation and the Holocene. *Paleoceanography*, *3*, 317–341. https://doi.org/10.1029/PA003i003p00317

Curry, W. B., & Oppo, D. (2005). Glacial water mass geometry and the distribution of $\delta^{13}C$ of ΣCO_2 in the western Atlantic Ocean. *Paleoceanography*, *20*, PA1017. https://doi.org/1010.1029/2004PA001021

Denton, G. H., Anderson, R. F., Toggweiler, J. R., Edwards, R. L., Schaefer, J. M., & Putnam, A. E. (2010). The Last Glacial Termination. *Science*, *328*, 1652–1656.

Duplessy, J.-C., Labeyrie, L., & Waelbroeck, C. (2002). Constraints on the ocean oxygen isotopic enrichment between the Last Glacial Maximum and the Holocene: Paleoceanographic implications. *Quaternary Science Reviews*, *21*(315–330), 315–330.

Duplessy, J.-C., Shackleton, N. J., Matthews, R. K., Prell, W. L., Ruddiman, W. F., Caralp, M., & Hendy, C. (1984). ^{13}C record of benthic foraminifera in the last interglacial ocean: Implications for the carbon cycle and the global deep water circulation. *Quaternary Research*, *21*, 225–243.

Elderfield, H., Ferretti, P., Greaves, M., Crowhurst, S., McCave, I. N., Hodell, D., & Piotrowski, A. M. (2012). Evolution of ocean temperature and ice volume through the mid-Pleistocene climate transition. *Science*, *337*, 704–709.

Elderfield, H., Greaves, M., Barker, S., Hall, I. R., Tripati, A., Ferretti, P., … Daunt, C. (2010). A record of bottom water temperature and seawater $\delta^{18}O$ for the Southern Ocean over the past 440 kyr based on Mg/Ca of benthic foraminiferal *Uvigerina* spp. *Quaternary Science Reviews*, *29*, 160–169.

Elmore, A. C. (2009). *Late Pleistocene changes in northern component water: Inferences from geochemical and sedimentological records from Gardar Drift* (Doctoral dissertation). Retrieved from https://doi.org/10.7282/T3VT1SBH

Ferrari, R., Jansen, M. F., Adkins, J. F., Burke, A., Stewart, A. L., & Thompson, A. F. (2014). Antarctic sea ice control on ocean circulation in present and glacial climates. *Proceedings of the National Academy of Sciences*, *111*(24), 8753–8758.

Galbraith, E. D., Kwon, E. Y., Bianchi, D., Hain, M. P., & Sarmiento, J. L. (2015). The impact of atmospheric pCO_2 on carbon isotope ratios of the atmosphere and ocean. *Global Biogeochemical Cycles*, *29*, 307–324. https://doi.org/10.1002/2014GB004929

Gersonde, R., Crosta, X., Abelmann, A., & Armand, L. (2005). Sea-surface temperature and sea ice distribution of the Southern Ocean at the EPILOG Last Glacial Maximum—A circum-Antarctic view based on siliceous microfossil records. *Quaternary Science Reviews*, *24*(7–9), 869–896.

Gherardi, J.-M., Labeyrie, L., Nave, S., Francois, R., McManus, J. F., & Cortijo, E. (2009). Glacial-interglacial circulation changes inferred from $^{231}Pa/^{230}Th$ sedimentary record in the North Atlantic region. *Paleoceanography*, *24*, PA2204. https://doi.org/10.1029/2008PA001696

Gruber, N., Keeling, C. D., Bacastow, R. B., Guenther, P. R., Lueker, T. J., Wahlen, M., … Stocker, T. F. (1999). Spatiotemporal patterns of carbon-13 in the global surface oceans and the oceanic Suess effect. *Global Biogeochemical Cycles*, *13*, 307–335. https://doi.org/10.1029/1999GB900019

Hertzberg, J. E., Lund, D. C., Schmittner, A., & Skrivanek, A. L. (2016). Evidence for a biological pump driver of atmospheric CO_2 rise during Heinrich Stadial 1. *Geophysical Research Letters*, *43*, 12,242–212,251. https://doi.org/10.1002/2016GL070723

Hillenbrand, C.-D., Kuhn, G., Smith, J. A., Gohl, K., Graham, A. G. C., Larter, R. D., … Vaughan, D. G. (2013). Grounding-line retreat of the West Antarctic Ice Sheet from inner Pine Island Bay. *Geology*, *41*(1), 35–38.

Hodell, D. A., Venz, K. A., Charles, C. D., & Ninnemann, U. S. (2003). Pleistocene vertical carbon isotope and carbonate gradients in the South Atlantic sector of the Southern Ocean. *Geochemistry, Geophysics, Geosystems*, *4*(1), 1004. https://doi.org/10.1029/2002GC000367

Hoffman, J. L., & Lund, D. C. (2012). Refining the stable isotope budget for Antarctic Bottom Water: New foraminiferal data from the abyssal southwest Atlantic. *Paleoceanography*, *27*, PA1213. https://doi.org/10.1029/2011PA002216

Howard, W. R., & Prell, W. L. (1992). Late Quaternary surface circulation of the Southern Indian Ocean and its relationship to orbital variations. *Paleoceanography*, *7*, 79–118. https://doi.org/10.1029/91PA02994

Hu, R., Noble, T. L., Piotrowski, A. M., NicholasMcCave, I., Bostock, H. C., & Neil, H. L. (2016). Neodymium isotopic evidence for linked changes in Southeast Atlantic and Southwest Pacific circulation over the last 200 kyr. *Earth and Planetary Science Letters*, *455*, 106–114.

Jaccard, S. L., Galbraith, E. D., Martínez-García, A., & Anderson, R. F. (2016). Covariation of deep Southern Ocean oxygenation and atmospheric CO_2 through the last ice age. *Nature*, *530*, 207–210.

Keigwin, L. D., & Swift, S. A. (2017). Carbon isotope evidence for a northern source of deep water in the glacial western North Atlantic. *Proceedings of the National Academy of Science*, *114*(11), 2831–2835.

Lamy, F., Arz, H. W., Kilian, R., Lange, C. B., Lembke-Jene, L., Wengler, M., … Tiedemann, R. (2015). Glacial reduction and millennial-scale variations in Drake Passage throughflow. *Proceedings of the National Academy of Sciences*, *112*(44), 13,496–13,501.

LeGrande, A. N., & Schmidt, G. A. (2006). Global gridded data set of the oxygen isotopic composition in seawater. *Geophysical Research Letters*, *33*, L12604. https://doi.org/10.1029/2006GL026011

Lowe, D. J., Blaauw, M., Hogg, A. G., & Newnham, R. W. (2013). Ages of 24 widespread tephras erupted since 30,000 years ago in New Zealand, with re-evaluation of the timing and palaeoclimatic implications of the Lateglacial cool episode recorded at Kaipo bog. *Quaternary Science Reviews*, *74*, 170–194.

Lund, D. C., Adkins, J., & Ferrari, R. (2011). Abyssal Atlantic circulation during the Last Glacial Maximum: Constraining the ratio between transport and vertical mixing. *Paleoceanography*, *26*, PA1213. https://doi.org/1210.1029/2010PA001938

Lund, D. C., Tessin, A. C., Hoffman, J. L., & Schmittner, A. (2015). Southwest Atlantic watermass evolution during the last deglaciation. *Paleoceanography*, *30*, 477–494. https://doi.org/10.1002/2014PA002657

Lynch-Stieglitz, J., Adkins, J. F., Curry, W. B., Dokken, T., Hall, I. R., Herguera, J. C., … Zahn, R. (2007). Atlantic Meridional Overturning Circulation during the Last Glacial Maximum. *Science*, *316*, 66–69.

Lynch-Stieglitz, J., Fairbanks, R. G., & Charles, C. D. (1994). Glacial-interglacial history of Antarctic Intermediate Water: Relative strengths of Antarctic versus Indian Ocean sources. *Paleoceanography*, *9*, 7–29. https://doi.org/10.1029/93PA02446

Mackensen, A. (2012). Strong thermodynamic imprint on recent bottom-water and epibenthic $\delta^{13}C$ in the Weddell Sea revealed: Implications for glacial Southern Ocean ventilation. *Earth and Planetary Science Letters*, *317-318*(C), 20–26.

Mackensen, A., Hubberten, H. W., Bickert, T., Fischer, G., & Fütterer, D. K. (1993). The $\delta^{13}C$ in benthic foraminiferal tests of *Fontbotia wuellerstorfi* (Schwager) relative to the $\delta^{13}C$ of dissolved inorganic carbon in Southern Ocean deep water: Implications for glacial ocean circulation models. *Paleoceanography*, *8*, 587–610. https://doi.org/10.1029/93PA01291

Marcott, S. A., Bauska, T. K., Buizert, C., Steig, E. J., Rosen, J. L., Cuffey, K. M., … Brook, E. J. (2014). Centennial-scale changes in the global carbon cycle during the last deglaciation. *Nature*, *514*, 616–619.

Marshall, D. P., Ambaum, M. H. P., Maddison, J. R., Munday, D. R., & Novak, L. (2017). Eddy saturation and frictional control of the Antarctic Circumpolar Current. *Geophysical Research Letters*, *44*, 286–292. https://doi.org/10.1002/2016GL071702

Marshall, J., & Speer, K. (2012). Closure of the meridional overturning circulation through Southern Ocean upwelling. *Nature Geoscience*, *5*, 171–180.

Matsumoto, K., & Lynch-Stieglitz, J. (1999). Similar glacial and Holocene deep water circulation inferred from southeast Pacific benthic foraminiferal carbon isotope composition. *Paleoceanography*, *14*, 149–163. https://doi.org/10.1029/1998PA900028

McCartney, M. S. (1977). Subantarctic mode water. In M. V. Angel (Ed.), *A Voyage of Discovery* (*Deep-Sea Research supplement*) (pp. 103–119). Oxford, UK: Pergammon.

McCave, I. N., Carter, L., & Hall, I. R. (2008). Glacial–interglacial changes in water mass structure and flow in the SW Pacific Ocean. *Quaternary Science Reviews*, *17*, 1886–1908.

McCave, I. N., Crowhurst, S., Kuhn, G., Hillenbrand, C.-D., & Meredith, M. (2014). Minimal change in Antarctic Circumpolar Current flow speed between the last glacial and Holocene. *Nature Geoscience*, *11*(7), 113–116.

McCorkle, D. C., & Keigwin, L. D. (1994). Depth profiles of $\delta^{13}C$ in bottom water and core-top *C. wuellerstorfi* on the Ontong Java Plateau and Emperor Seamounts. *Paleoceanography*, *9*, 197–208. https://doi.org/10.1029/93PA03271

McManus, J. F., Francois, R., Gherardi, J. M., Keigwin, L. D., & Leger, S. B. (2004). Collapse and rapid resumption of Atlantic meridional circulation linked to deglacial climate changes. *Nature*, *428*, 834–837.

Ninnemann, U. S., & Charles, C. D. (2002). Changes in the mode of Southern Ocean circulation over the last glacial cycle revealed by foraminiferal stable isotopic variability. *Earth and Planetary Science Letters*, *201*, 383–396.

Oppo, D. W., Curry, W. B., & McManus, J. (2015). What do benthic $\delta^{13}C$ and $\delta^{18}O$ data tell us about Atlantic circulation during Heinrich Stadial 1? *Paleoceanography*, *30*, 353–368. https://doi.org/10.1002/2014PA002667

Oppo, D. W., & Fairbanks, R. G. (1987). Variability in the deep and intermediate water circulation of the Atlantic Ocean during the past 25,000 years: Northern Hemisphere modulation of the Southern Ocean. *Earth and Planetary Science Letters*, *86*, 1–15.

Orsi, A., Whitworth, T., & Nowlin, W. D. (1995). On the meridional extent and fronts of the Antarctic Circumpolar Current. *Deep Sea Research*, *42*, 641–673.

Orsi, A. H., Johnson, G. C., & Bullister, J. L. (1999). Circulation, mixing, and production of Antarctic bottom water. *Progress in Oceanography*, *43*, 55–109.

Peeters, F. J. C., Acheson, R., Brummer, G.-J. A., Ruijter, W. P. M. D., Schneider, R. R., Ganssen, G. M., … Kroon, D. (2004). Vigorous exchange between the Indian and Atlantic oceans at the end of the past five glacial periods. *Nature*, *430*, 661–665.

Praetorius, S. K., McManus, J. F., Oppo, D. W., & Curry, W. B. (2008). Episodic reductions in bottom-water currents since the last ice age. *Nature Geoscience*, *1*(7), 449–452.

Putnam, A. E., Schaefer, J. M., Denton, G. H., Barrell, D. J. A., Birkel, S. D., … Doughty, A. L. (2013). The Last Glacial Maximum at 44°S documented by a ^{10}Be moraine chronology at Lake Ohau, Southern Alps of New Zealand. *Quaternary Science Reviews*, *62*(C), 114–141.

Reimer, P. J., Bard, E., Bayliss, A., Beck, J. W., Blackwell, P. G., Ramsey, C. B., … van der Plicht, J. (2013). IntCal13 and MARINE13 radiocarbon age calibration curves 0–50000 years cal BP. *Radiocarbon*, *55*(4). https://doi.org/10.2458/azu_js_rc.2455.16947

Rickaby, R. E. M., & Elderfield, H. (2005). Evidence from the high-latitude North Atlantic for variations in Antarctic Intermediate water flow during the last deglaciation. *Geochemistry, Geophysics, Geosystems*, *6*, Q05001. https://doi.org/10.1029/2004GC000858

Roberts, J., Gottschalk, J., Skinner, L. C., Peck, V. L., Kender, S., Elderfield, H., … Hodell, D. A. (2015). Evolution of South Atlantic density and chemical stratification across the last deglaciation. *PNAS*, *113*(3), 514–519.

Ronge, T. A., Tiedemann, R., Lamy, F., Köhler, P., Alloway, B. V., Pol-Holz, R. D., … Wacker, L. (2016). Radiocarbon constraints on the extent and evolution of the South Pacific glacial carbon pool. *Nature Comminications*, 11. https://doi.org/10.1038/ncomms11487

Rutberg, R. L., Hemming, S. R., & Goldstein, S. L. (2000). Reduced North Atlantic Deep Water flux to the glacial Southern Ocean inferred from neodymium isotope ratios. *Nature*, *405*, 935–938.

Sallée, J. B., Speer, K. G., & Rintoul, S. R. (2010). Zonally asymmetric response of the Southern Ocean mixed layer depth to the Southern Annular Mode. *Nature Geoscience*, *3*, 273–279.

Samson, C. R., Sikes, E. L., & Howard, W. R. (2005). Deglacial paleoceanographic history of the Bay of Plenty, New Zealand. *Paleoceanography*, *20*, PA4017. https://doi.org/10.1029/2004PA001088

Sarmiento, J. L., Gruber, N., Brzezinski, M. A., & Dunne, J. P. (2004). High latitude controls on thermocline nutrients and low latitude biological productivity. *Nature*, *427*, 56–60.

Sarnthein, M., Schneider, B., & Grootes, P. M. (2013). Peak glacial ^{14}C ventilation ages suggest major draw-down of carbon into the abyssal ocean. *Climate of the Past*, *9*, 2595–2614.

Schmittner, A., Gruber, N., Mix, A. C., Key, R. M., Tagliabue, A., & Westberry, T. K. (2013). Biology and air-sea gas exchange controls on the distribution of carbon isotope ratios ($\delta^{13}C$) in the ocean. *Biogeosciences*, *10*, 5793–5816.
Schmittner, A., & Lund, D. C. (2015). Early deglacial Atlantic overturning decline and its role in atmospheric CO_2 rise inferred from carbon isotopes ($\delta^{13}C$). *Climate of the Past*, *1*, 135–152.
Shackleton, N. J. (1967). Oxygen isotope analyses and Pleistocene temperatures re-assessed. *Nature*, *215*, 15–17.
Shane, P. A., Sikes, E. L., & Guilderson, T. P. (2006). Tephra beds in deep-sea cores off northern New Zealand: Implications for the history of Taupo Volcanic Zone, Mayor Island, and White Island volcanoes. *Journal of Volcanic and Geothermal Research*, *154*(4), 276–290.
Sigman, D. M., Hain, M. P., & Haug, G. H. (2010). The polar ocean and glacial cycles in atmospheric CO_2 concentration. *Nature*, *466*, 47–55.
Sikes, E. L., & Guilderson, T. P. (2016). Southwest Pacific Ocean surface reservoir ages since the last glaciation: Circulation insights from multiple-core studies. *Paleoceanography*, *31*, 298–310. https://doi.org/10.1002/2015PA002855
Sikes, E. L., Cook, M. S., & Guilderson, T. P. (2016). Reduced deep ocean ventilation in the Southern Pacific Ocean during the last glaciation persisted into the deglaciation. *Earth and Planetary Science Letters*, *438*, 130–138.
Sikes, E. L., Elmore, A. C., Cook, M. S., Allen, K. A., & Guilderson, T. P. (2016). Glacial water mass structure and rapid $\delta^{18}O$ and $\delta^{13}C$ changes during the last glacial termination in the Southwest Pacific. *Earth and Planetary Science Letters*, *456*, 87–97.
Sikes, E. L., Howard, W. R., Samson, C. R., Mahan, T. S., Robertson, L. G., & Volkman, J. K. (2009). Southern Ocean seasonal temperature and Subtropical Front movement on the South Tasman Rise in the Late Quaternary. *Paleoceanography*, *24*, PA2201. https://doi.org/10.1029/2008PA001659
Sikes, E. L., Samson, C. R., Guilderson, T. P., & Howard, W. R. (2000). Old radiocarbon ages in the southwest Pacific Ocean during the last glacial period and deglaciation. *Nature*, *405*, 555–559.
Skinner, L., McCave, I. N., Carter, L., Fallon, S., Scrivner, A. E., & Primeaud, F. (2015). Reduced ventilation and enhanced magnitude of the deep Pacific carbon pool during the last glacial period. *Earth and Planetary Science Letters*, *411*, 45–52.
Stern, J. V., & Lisiecki, L. E. (2014). Termination 1 timing in radiocarbon-dated regional benthic $\delta^{18}O$ stacks. *Paleoceanography*, *29*, 1127–1142. https://doi.org/10.1002/2014PA002700
Takahashi, T., Sutherland, S. C., Wanninkhof, R., Sweeney, C., Feely, R. A., … de Baar, H. J. W. (2009). Climatological mean and decadal change in surface ocean pCO_2, and net sea–air CO_2 flux over the global oceans. *Deep Sea Research Part II: Topical Studies in Oceanography*, *56*(8–10), 554–577.
Talley, L. (2013). Closure of the global overturning circulation through the Indian, Pacific, and Southern Oceans: Schematics and transports. *Oceanography*, *26*(1), 80–97.
Tessin, A. C., & Lund, D. C. (2013). Isotopically depleted carbon in the mid-depth South Atlantic during the last deglaciation. *Paleoceanography*, *28*, 296–306. https://doi.org/10.1002/palo.20026
Thornalley, D. J. R., McCave, I. N., & Elderfield, H. (2010). Freshwater input and abrupt deglacial climate change in the North Atlantic. *Paleoceanography*, *25*, PA1201. https://doi.org/10.1029/2009PA001772
Toggweiler, J. R. (1999). Variation of atmospheric CO_2 by ventilation of the ocean's deepest water. *Paleoceanography*, *14*, 571–588. https://doi.org/10.1029/1999PA900033
Toggweiler, J. R., & Samuels, B. (1995). Effect of Drake Passage on the global thermohaline circulation. *Deep Sea Research, Part I*, *42*, 477–500.
Ullermann, J., Lamy, F., Ninnemann, U., Lembke-Jene, L., Gersonde, R., & Tiedemann, R. (2016). Pacific-Atlantic Circumpolar Deep Water coupling during the last 500 ka. *Paleoceanography*, *31*, 639–650. https://doi.org/10.1002/2016PA002932
Vandergoes, M. J., Hogg, A. G., Lowe, D. J., Newnham, R. M., Denton, G. H., Southon, J. R., … Blaauw, M. (2013). A revised age for the Kawakawa/Oruanui tephra, a key marker for the Last Glacial Maximum in New Zealand. *Quaternary Science Reviews*, *74*(1–7), 195–201.
Warren, B. A. (1990). Suppression of deep oxygen concentrations by Drake Passage. *Deep Sea Research*, *37*, 1899–1907.
Wolff, E. W., Fischer, H., Fundel, F., Ruth, U., Twarloh, B., Littot, G., … Gaspari, V. (2006). Southern Ocean sea-ice extent, productivity and iron flux over the past eight glacial cycles. *Science*, *440*, 491–496.
Yu, J., Elderfield, H., & Piotrowski, A. M. (2008). Seawater carbonate ion-$\delta^{13}C$ systematics and application to glacial-interglacial North Atlantic ocean circulation. *Earth and Planetary Science Letters*, *271*, 209–220.